Opto-Electronic Advances

Supplementary information

October 2023, Vol. 6, No. 10

DOI: 10.29026/oea.2023.230076

Knot-inspired optical sensor for slip detection and friction measurement in dexterous robotic manipulation

Jing Pan[1], Qi Wang[1], Shuaikang Gao[1], Zhang Zhang[1], Yu Xie[1], Longteng Yu[1]* and Lei Zhang[1,2]*

[1]Research Center for Humanoid Sensing, Zhejiang Lab, Hangzhou 311100, China; [2]State Key Laboratory of Modern Optical Instrumentation, College of Optical Science and Engineering, Zhejiang University, Hangzhou 310027, China.

*Correspondence: LT Yu, E-mail: ylt@zhejianglab.edu.cn; L Zhang, E-mail: zhang_lei@zju.edu.cn

This file includes:

Supplementary information for this paper is available at https://doi.org/10.29026/oea.2023.230076

Section 1: Fabrication of the flat OFN sensors

An OFN sensor is made by encapsulating an OFN in a PDMS block. The block can be either a cube or a slab. In both cubic and flat OFN sensors, the OFN is positioned at the midplane of the PDMS block. The step-by-step fabrication flow is illustrated in Fig. S4. Step I: Fabricate a negative mold made of resin (DSM Somos® 8100 Epoxy Photopolymer) through 3D printing. Step II: Fill the degassed PDMS pre-polymer (base to agent ratio is 10:1) into the negative mold, and heat up to 60 °C for 30 minutes to cure. Step III: Remove the cured PDMS piece from the negative mold to obtain positive molds. Each PDMS positive mold consists of a square base and a cylindrical pillar positioned at the center. The diameter of the pillar is 1 mm less than the side length of the base. Step IV: Place an OFN around the pillar and fasten it by pulling the two fiber tails. The knot is fixed at the bottom of the pillar. Step V: Transfer the fastened OFN along with the PDMS mold into a resin holder. Fill it with degassed PDMS and heat it up to cure. Step VI: Demold to obtain an OFN sensor.

Section 2: Fabrication of the cubic OFN sensors

Similar to the flat OFN sensor, the fabrication process of the cubic OFN sensor also involves the use of a PDMS mold to regulate the size of the fiber knot and its positioning within the cube. Fig. S5 demonstrates that the diameter d_0 of the cylindrical pillar corresponds to the inner circle diameter of the knot, while the thickness of the square base determines the knot's placement at the midplane of the cube.

Section 3: Materials of the OFN sensors

It is worth noting that the majority of polymer optical fibers can be utilized as raw materials for fabricating fiber knot sensors. The primary reason for us to choose PMMA fibers is that they are easily accessible, inexpensive, and flexible. The superior flexibility of the PMMA fibers to standard silica fibers allows us to readily make a knot with a tiny footprint without delicate operation and sophisticated instruments. Besides, the cladding of PMMA optical fibers ensures total internal reflection and prevents light coupling between two fibers when they come into contact. This feature simplifies the analysis of the sensor and reduces measurement complexity.

The encapsulation of the knot plays a crucial role in protecting the sensing element and transmitting external forces. We chose PDMS due to its advantages such as easy accessibility, cost-effectiveness and flexibility. Other polymers can also be implemented in fabricating OFN sensors using our proposed method. In addition to PDMS, we recommend other silicones such as Ecoflex, and Dragon Skin series, which are commonly employed in various soft and flexible sensors.

We compared the response of PMMA OFNs to normal force with and without the PDMS encapsulation (see Fig. S1). It can be observed that the PDMS encapsulation significantly expands the sensor's dynamic working range while also reducing its sensitivity. In fact, the choice of coating material could effectively adjust the sensor's response to external forces. The selection of fiber and coating materials can be tailored to meet specific requirements.

Section 4: Coupling method of the fiber and the LED

The coupling between the fiber and the LED was achieved via a customized fixture (Fig. S3). The fixture encloses the head of the LED, and the input end of the fiber. The fixture is made from opaque plastic materials, to avoid influence from ambient light. In the fixture, the input end of the optical fiber is directly in contact with the top of the LED.

Section 5: Finite element simulations of OFN under normal and frictional forces

We implemented Finite Element Method (FEM) to calculate the stress and strain distribution of a flat OFN sensor under normal and frictional forces in COMSOL Multiphysics. The PMMA fiber thickness was 250 μm and the thickness of the PDMS slab was 1 mm. The materials of fiber and cladding were assumed to be PMMA (Young's modulus: 3.7 GPa, Poisson's ratio: 0.37, density: 1150 kg/m^3) and PDMS (Young's modulus: 2.05 MPa, Poisson's ratio: 0.47, density: 950 kg/m^3), respectively. A normal force of 10 N and a frictional force of 4 N were applied on the top surface of the sensor. The numerical results of OFN sensors with knot diameters of 4.5 mm, 3.5 mm, and 2.5 mm are shown in Movie S1. The strain distribution of the OFN sensor with a knot diameter of 3.5 mm is illustrated in Fig. 1(f–h).

Section 6: Data acquisition and processing

To investigate the static and dynamic responses of OFN sensors, broadband light from a tungsten halide lamp (SLS201L, Thorlabs, USA) was coupled into the optical fiber (250 μm, PMMA Fiber) and served as the probing light. The transmitted light was recorded by a spectrometer (Maya2000 Pro, Ocean Optics, USA). For the characterization of the flat OFN sensor and the robotic tactile finger, we employed an LED (TJ-L3FYTGHTCGSFLC0A-A5, Togialed, Taiwan, China) as the light source and a PD (PD333-3C-H0-L2, Everlight, Taiwan, China) as the receptor.

Normal and frictional forces were applied to the flat OFN sensor by a metal probe. The probe was driven by a tri-axial motorized stage (M-462-3, Newport, USA). Reference force was recorded by a six-axis force/torque sensor (Nano17, ATI Industrial Automation, USA).

Tri-axial forces on the cubic OFN sensor were applied by a programmable single-column mechanical tester (ESM303, Mark-10, USA), and recorded by a digital force gauge (Model 5i, Mark-10, USA).

Section 7: Slip detection program

Our customized slip detection program, Slip Finder, was built based on Change Finder, a real-time change point detection (CPD) algorithm described in ref.[S1]. As the name suggests, a CPD algorithm detects abrupt variations, i.e., change points, in a data sequence. In the signal of an OFN sensor, an abrupt change can be either a spike caused by a slip or a step caused by a pressure jump. Hence, another scheme must be employed to differentiate between spikes and steps. Such scheme starts to monitor the intensity change once a change point is detected by Change Finder. We denote the intensity change at the change point as ΔI_0, and the intensity change after the change point as ΔI_t. In a spike, ΔI_t rapidly deviates from ΔI_0, whereas in a step, ΔI_t remains close to ΔI_0. By monitoring ΔI_t for a short time, we can determine whether the change point is a "slip point" or a "pressure point". In this way, a slip can be readily detected with Slip Finder in real time.

Section 8: Robotic experiments

A collaborative robotic arm (UR 3e, Universal Robots, Denmark) and a two-fingered robotic gripper (2f-85, Robotiq, Canada) were employed in our experiments. All robotic programs were run in the Robot Operating System (ROS). In the cup grasping experiment, the program regulated the Finger Position of the robotic gripper based on the feedback from Slip Finder. Slip Finder detects slip based on the sensing signals of the OFN sensors. Two flat OFN sensors were fixed on the same finger of the gripper and aligned with the finger direction. In the tofu-cutting and door-unlocking experiments, the original fingers were replaced by the customized robotic tactile fingers. Robotic programs controlled the maneuvers of both the arm and the gripper, based on the tri-axial force values measured by the tactile fingers.

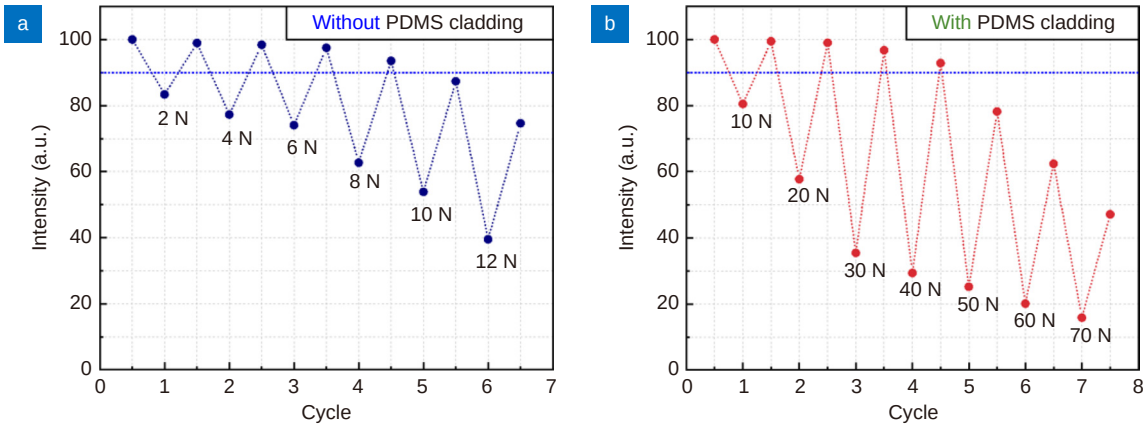

Fig. S1 | Responses of OFN sensors with and without PDMS cladding to normal force, respectively.

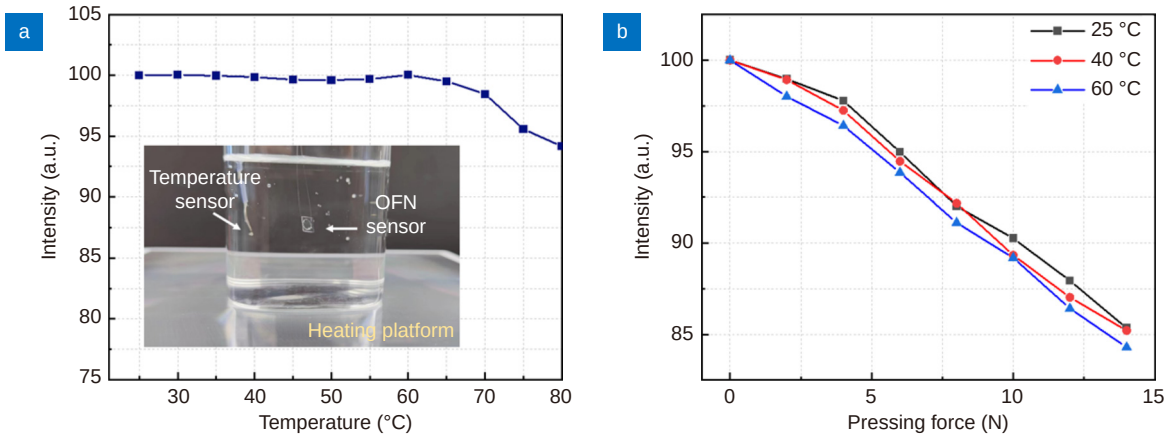

Fig. S2 | (**a**) Output intensity of an OFN sensor. (**b**) Response curves of the OFN sensor to pressing force under 25 °C, 40 °C and 60 °C.

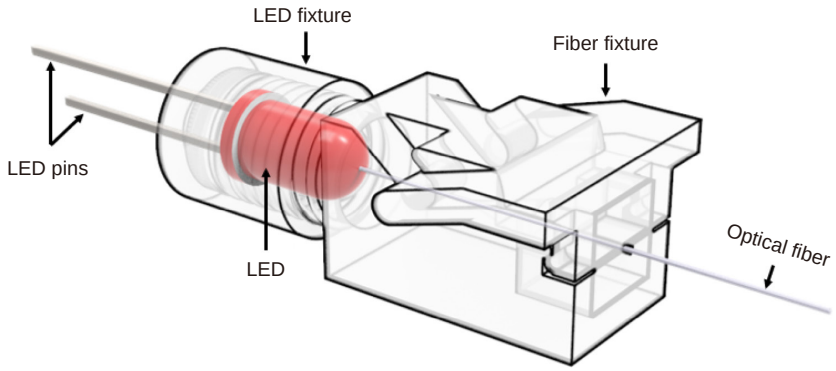

Fig. S3 | The schematic diagram of the LED-fiber coupling fixture.

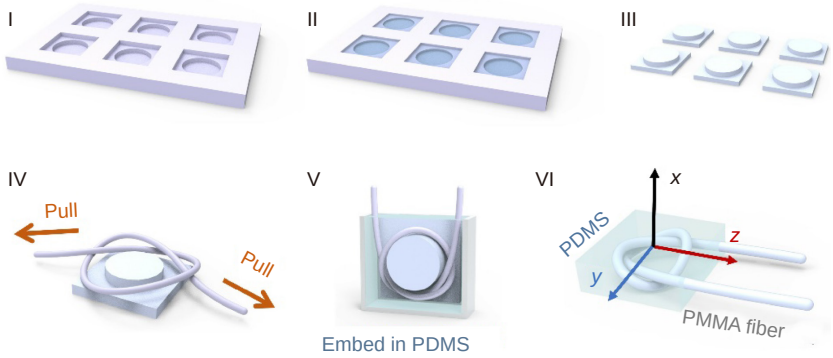

Fig. S4 | Fabrication process of the flat OFN sensor.

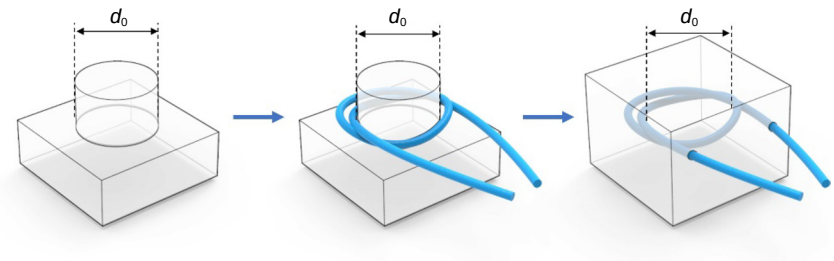

Fig. S5 | Fabrication process of the cubic OFN sensor.

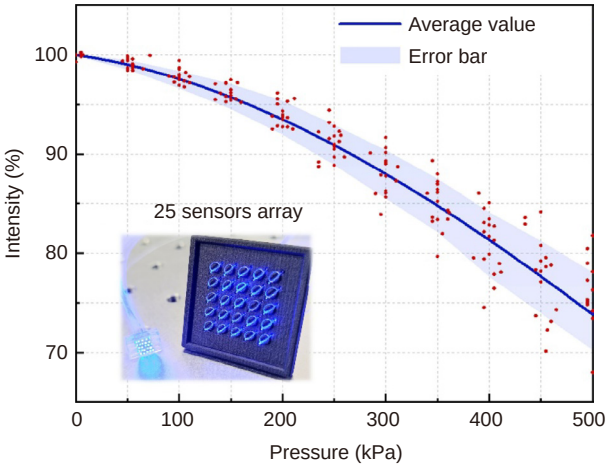

Fig. S6 | Pressure response of 25 individual OFN sensors in a sensing array.

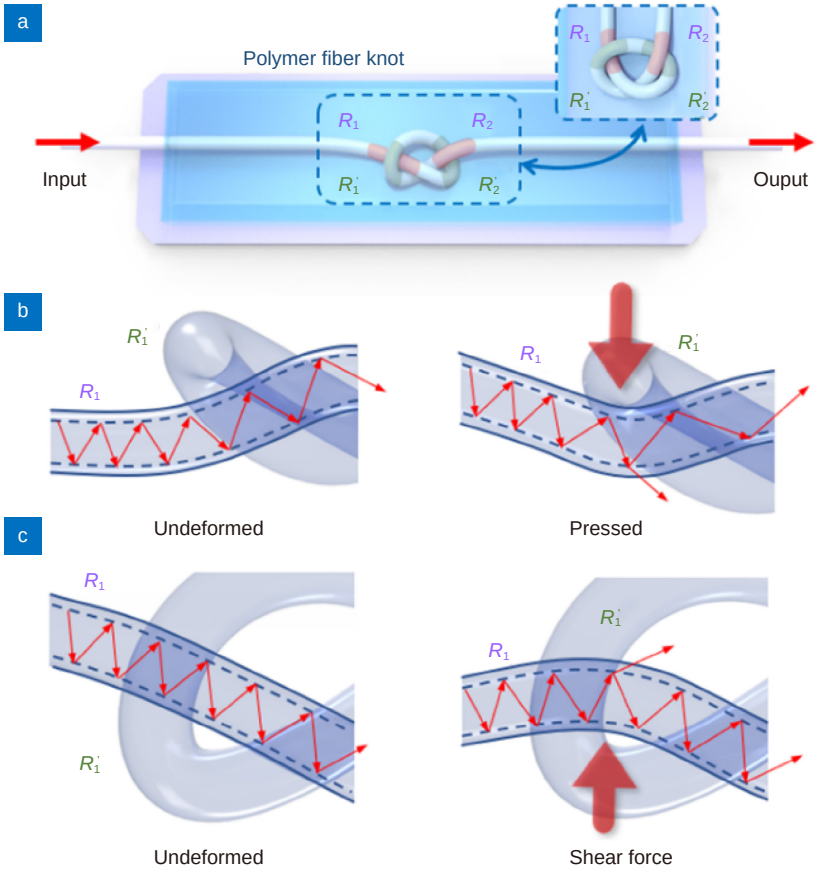

Fig. S7 | Ray diagrams of OFN when it is deformed by (**a**) a normal force and (**b**) a frictional force.

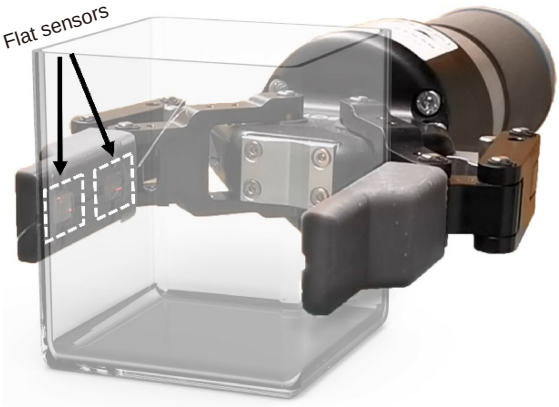

Fig. S8 | A two-fingered robotic gripper equipped with two flat OFN sensors.

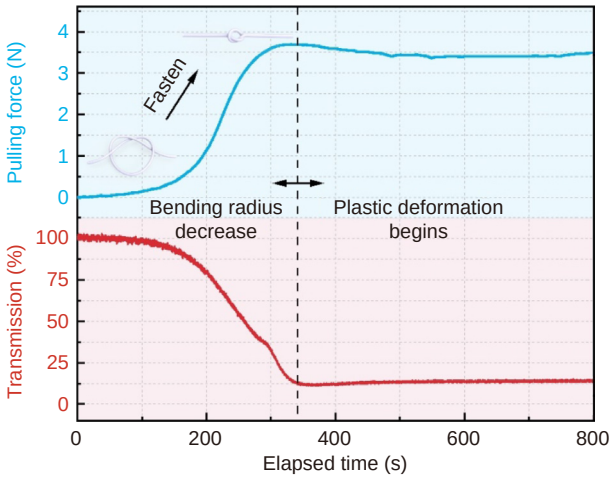

Fig. S9 | The transmission reduces as the OFN is stretched.

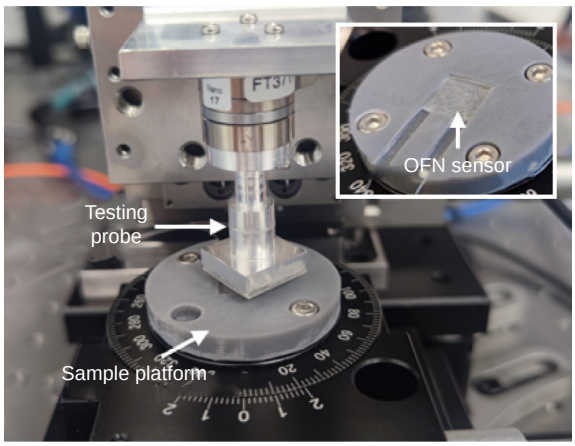

Fig. S10 | Photograph of the friction testing system.

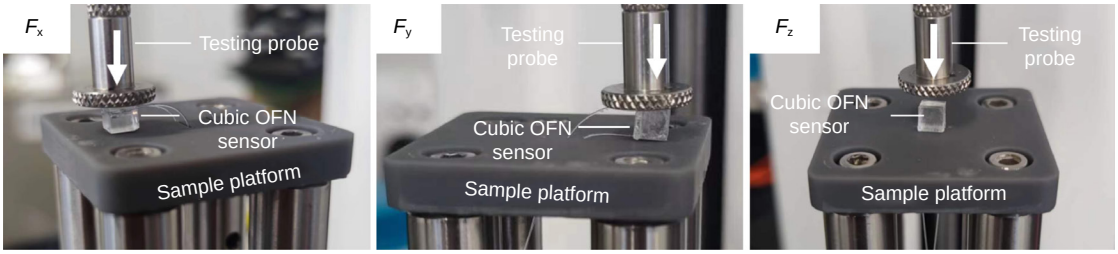

Fig. S11 | Photograph of the tri-axial force testing system.

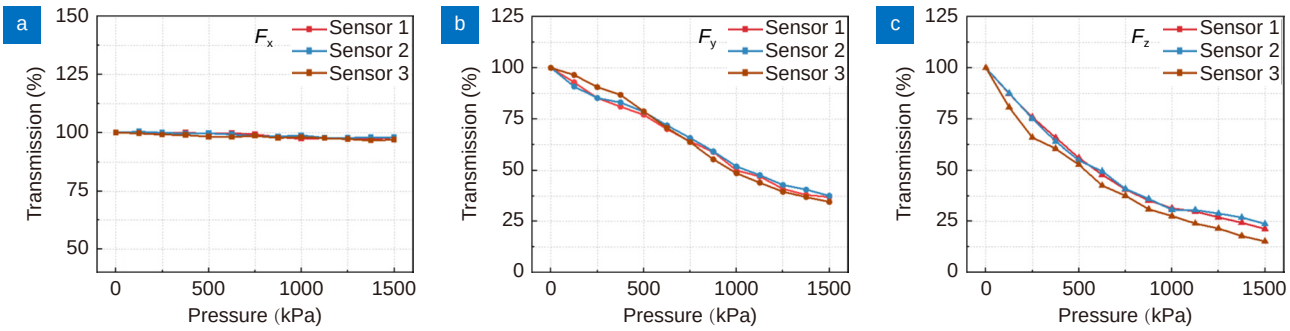

Fig. S12 | Responses of OFN sensors with knot diameters of 3.5 mm to F_x, F_y and F_z, respectively.

Movie S1 | Finite element simulations of OFN sensors under normal and frictional forces.

These numerical results show the stress and strain distribution of a flat OFN sensor with knot diameter of 4.5 mm, 3.5 mm, and 2.5 mm, respectively. A normal force of 10 N and a frictional force of 4 N were applied on the top surface of the sensor.

Movie S2 | A robotic gripper grasps a slipping cup via slip feedback based on OFN sensors.

We commanded a two-fingered robotic gripper to grasp a plastic cup. Two OFN sensors were attached on one finger pad to detect slip. The OFN sensors and a slip detection program comprised a slip detection system. When screws dropped into the cup, the robotic gripper closed further to suppress slipping.

Movie S3 | A robotic gripper fails to grasp a slipping cup when the slip feedback is off.

We cut the feedback from OFN sensors and repeated the adaptive grasping experiment. The robotic gripper was unable to adjust grasping force and failed to prevent the cup from dropping. Experiments shown in Movie S2 and Movie S3 validate that our slip detection system can effectively detect slip and assist adaptive robotic grasping.

Movie S4 | A robotic gripper uses a knife to cut tofu via tri-axial force sensing based on OFN sensors.

We integrated the tactile fingers into a robotic gripper. The robot gripped a knife and cut tofu three times. The force in all three directions was detected by the tactile finger during the cutting process.

Movie S5 | A robotic gripper uses a key to unlock a locker via tri-axial force sensing based on OFN sensors.

We commanded the robot integrated with the tactile fingers to unlock a locker with a key. The tri-axial force was detected by the tactile finger during the whole process.

References

S1. Takeuchi J, Yamanishi K. A unifying framework for detecting outliers and change points from time series. *IEEE Trans Knowl Data Eng* **18**, 482–492 (2006).